Image-Force-Stabilized Interfacial Dipole Layer Impedes Charge Injection Into Disordered Organic Semiconductors

Feilong Liu,[1,*] Yuhao Su,[1] Xihong Lin,[1] Li Nian,[1] Bo Wu,[1] Quan Niu,[5] Harm van Eersel,[4] Peter A. Bobbert,[2] Reinder Coehoorn,[1,2,†] and Guofu Zhou[1,3,‡]

[1] *Guangdong Provincial Key Laboratory of Optical Information Materials and Technology & Institute of Electronic Paper Displays, South China Academy of Advanced Optoelectronics, South China Normal University, Guangzhou 510006, People's Republic of China*

[2] *Department of Applied Physics and Institute for Complex Molecular Systems, Eindhoven University of Technology, Eindhoven University of Technology, P.O. Box 513, MB Eindhoven 5600, Netherlands*

[3] *Shenzhen Guohua Optoelectronics Tech. Co. Ltd., Shenzhen 518110, People's Republic of China*

[4] *Simbeyond B.V., Het Eeuwsel 57, AS Eindhoven 5612, Netherlands*

[5] *State Key Laboratory of Luminescent Materials and Devices, South China University of Technology, Guangzhou 510640, People's Republic of China*

(Received 30 November 2020; revised 19 November 2021; accepted 7 January 2022; published 1 February 2022)

We show using three-dimensional kinetic Monte Carlo simulations that the injection of charge carriers from a metallic electrode into a disordered organic semiconductor is under nominally Ohmic injection conditions strongly impeded by the short-range Coulomb interactions between the charge carriers in the image-force-stabilized interfacial dipole layer. In contrast, master equation and conventional one-dimensional drift-diffusion simulations underestimate these Coulomb interactions due to their mean-field approximation, and are found not to reveal the effect. The simulations predict a reduction of the current density in organic semiconductor devices when the nominal injection barrier is taken very small or even negative, consistent with recent experimental results [Kotadiya *et al.*, Nat. Mater. **17**, 329 (2018)]. However, whereas in that work a modification of the energetic disorder near the interface is assumed, we find that the effect is already obtained after including charge-charge interactions beyond a one-dimensional and mean-field approximation.

DOI: 10.1103/PhysRevApplied.17.024003

I. INTRODUCTION

Charge-carrier injection from a metallic electrode into an intrinsic organic semiconductor is a key process in organic light-emitting diodes (OLEDs) and other organic electronic devices such as organic field-effect transistors (OFETs), organic solar cells, and organic photodetectors [1–12]. In OLEDs, strong efforts have been focused on reducing the efficiency loss resulting from injection barriers, for example, using thin interlayers [1,11] and molecularly doped injection layers [13–15]. It has long been known that the effective injection barrier is not simply given by the energy difference between the metal Fermi level and the relevant frontier orbital energy, as expressed by the electron affinity or the ionization energy for electron or hole injection, respectively. Extensive experimental [16–21] and device-theoretical [4,6,11,20–25] studies have revealed the formation of an interfacial electric dipole layer and have elucidated the effects on its formation of energetic disorder and the image-charge interaction. On the one hand, this thin high-carrier-density zone forms, at least within the framework of mean-field simulations, the high-conductivity reservoir of charge carriers that is required for obtaining ideal ("Ohmic") injection conditions. On the other hand, the formation of such an interfacial dipole layer, disadvantageously, increases the effective injection barrier.

Recently, Kotadiya *et al.* showed how this dilemma can be solved [11]. The authors found, firstly, that hole injection into various hole-transporting organic semiconductors from a high-work-function MoO_3 electrode is not Ohmic, in spite of a large negative nominal injection barrier. This was tentatively explained by postulating a broadened width of the Gaussian density of states (DOS) in a thin (2-nm) zone near the interface between the hole-transporting material and the electrode, reflecting enhanced structural disorder in that zone or resulting from the image-charge interaction. Results of photoemission studies, combined

*feilongliu@m.scnu.edu.cn
†r.coehoorn@tue.nl
‡guofu.zhou@m.scnu.edu.cn

with one-dimensional drift-diffusion simulations of the charge density near the interface, were found to be consistent with that analysis. The resulting enhanced charge density in the first organic layers will then lead to a positive injection barrier. Next, the authors showed that the injection can become Ohmic when inserting a thin interlayer with a high ionization energy [11,12]. This counterintuitive effect of a barrier layer was explained as a result of the reduced image potential stabilization of the charge density in the hole-transporting organic semiconductor, thereby effectively eliminating the injection barrier. It is not yet clear to what extent these observations are material specific, and related, for example, to a modified shape of the hole density of states near specific metal electrodes.

In this paper, we show from three-dimensional kinetic Monte Carlo (3D KMC) simulations that a distinct deviation from Ohmic injection is expected for *any* metal-organic system with a nominally negative injection barrier. The effect is shown to be a beyond-mean-field Coulomb effect, resulting from the Coulomb interaction between the injected charge carriers in the first layer of organic molecules, between the injected charge carriers and their image charges in the electrode, as well as the Coulomb repulsion impeding charge carriers being further injected into the second layer of molecular sites nearby. For disordered materials with localized charge carriers, a well-known consequence is the formation of a Coulomb glass [26,27]. KMC studies of the charge transport in the bulk of organic semiconductors [28,29] and in OFETs [30] show that a reduction of the mobility can indeed occur at large carrier concentrations ($> 10^{-3}$ per molecule), combined with small electric fields. Whereas such conditions, in general, do not occur in the interior of an OLED, we find here that accurate calculation of Coulomb interaction of the image-force-stabilized interfacial dipole layer is crucial for understanding the physics of the thin high-density interfacial zone. We furthermore show that also the elimination of the injection barrier using an interlayer, as studied in Ref. [11], is a generic effect, and use the 3D KMC simulations to investigate under well-controlled conditions how the interlayer can be optimally chosen.

The paper is structured as follows. Section II contains a description of the 3D kinetic Monte Carlo, 3D master equation, and 1D drift-diffusion simulation methods that have been used in this work. In Sec. III the simulation results are presented and discussed. Section IV summarizes the conclusions and gives and outlook to future next steps.

II. SIMULATION METHODS

The need to treat the Coulomb interaction between the charges near the injecting interface beyond a mean-field approach is demonstrated by comparing the current density in hole-only devices as obtained from 3D KMC simulations [31–33] with the results of mean-field simulations using the three-dimensional master equation (3D ME) [9,34,35] and continuous-medium one-dimensional drift-diffusion (1D DD) [36,37] methods. Within the 3D KMC and 3D ME simulations, the molecules are located on a simple cubic lattice with an intermolecular distance $a = 1$ nm. The HOMO energy at each molecular site is randomly drawn from a Gaussian distribution with a mean energy E_{HOMO} and a width (standard deviation) σ. The hole-hopping process from molecule i to j is described by the Miller-Abrahams rate [38]

TABLE I. Overview of material and device parameters.

Parameter	Value
Intermolecular distance a	1 nm
HOMO Gaussian distribution width σ	0.1 eV
Hopping-attempt frequency ν_1	3.3×10^{10} s^{-1}
Wave-function decay length λ	0.3 nm
Relative dielectric permittivity ε_r	3
Device thickness L	100 nm

$$\nu_{ij} = \nu_0 \exp\left(-\frac{2R_{ij}}{\lambda}\right) \exp\left(-\frac{|\Delta E_{ij}| + \Delta E_{ij}}{2k_B T}\right), \quad (1)$$

with R_{ij} the distance between molecular site i and j, ν_0 the hopping attempt frequency, λ the wave-function decay length, $\Delta E_{ij} = E_j - E_i$ the energy difference between sites j and i, k_B the Boltzmann constant, and T the temperature. The metallic electrodes are assumed to be perfectly screening, so that the electric field vanishes inside the electrode. The 3D Coulomb potential around each individual charge carrier is at all neighbors within a distance of $R_C = 10$ nm included in an exact manner. The dielectric screening due to the thin-film environment is described by a distance-independent relative dielectric permittivity ε_r. The Coulomb interaction with more distant charges is calculated by solving a one-dimensional Poisson equation based on the layer-averaged charge-carrier density [39]. The results presented in this paper do not change when increasing R_C. The site energies include the intrinsic Gaussian disorder, the electrostatic energy due to the applied voltage, the Coulomb interaction energy with the other charge carriers, and the image-charge reduction as described in Ref. [39]. The rates of the charge injection and collection processes are described by a Miller-Abrahams-type expression that is analogous to Eq. (1), with a spatial decay determined by the distance R_i from the molecular site i to the nearby electrode and the energy changes for injection and collection equal to $E_i - E_F$ and $E_F - E_i$, respectively, with E_F the Fermi energy of the electrode.

We note that it is not *a priori* evident that KMC simulations for systems with a small or negative injection barrier, and hence with a large Coulomb-correlated charge-carrier density near the injecting interface, provide within a

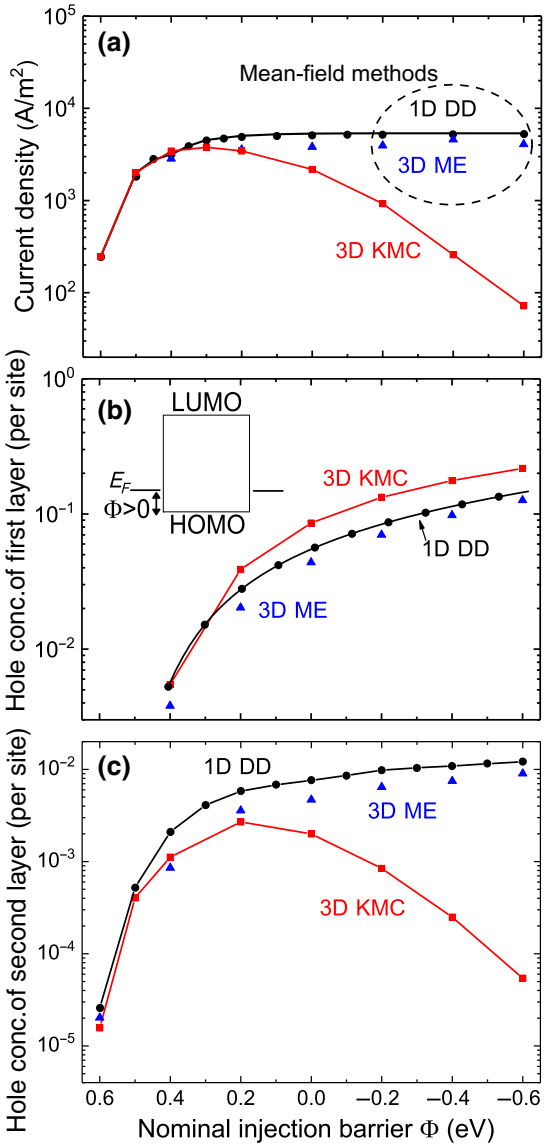

FIG. 1. Current density (a) and hole concentration (holes per molecular site) in the first (b) and second (c) molecular layers adjacent to the injecting electrode in a hole-only metal-OS-metal device at 5 V and 290 K, studied as a function of the nominal injection barrier Φ using 3D KMC, 3D ME, and 1D DD modeling, for the material and device parameters given in Table I. Φ is defined in the inset of (b).

realistic simulation time a well-equilibrated dynamic equilibrium state. We have therefore carefully carried out the simulations for a sufficiently large total device area, to eliminate possible disorder-induced fluctuations, and for a sufficiently large time, until the uncertainty in the calculated current density is smaller than the symbol size in the figures.

As a second reference, we use the continuous-medium 1D DD simulation method that has been described in Ref. [37], employing a charge-carrier density and electric field dependence of the mobility that is consistent with the results of 3D KMC simulations, and employing the generalized Einstein equation to deduce the diffusion coefficient from the mobility [40]. The charge-carrier density and electric field boundary conditions at the metal interfaces include the image-charge effect as described within the Emtage-O'Dwyer model [41]. An overview of details of the simulation methods used is given in Sec. S1 of the Supplemental Material [42].

III. RESULTS AND DISCUSSION

A. Single-layer devices

We first focus on 100-nm-thick hole-only sandwich-type devices, formed by a single disordered organic semiconductor (OS) layer in between two identical metallic electrodes. Figure 1(a) shows the dependence of the current density on the nominal injection barrier $\Phi \equiv E_F - E_{\mathrm{HOMO}}$, obtained at 5 V and at 290 K using the three simulation methods introduced above and using a set of material parameters that is representative of disordered organic semiconductors (see Table I). From the 3D KMC simulations, the current density is found to show a clear maximum for $\Phi \sim 0.3$ eV. For larger injection barriers, the two mean-field methods agree well with the 3D KMC results. The effective injection barriers and boundary conditions are then adequately included in the mean-field methods. However, for smaller injection barriers, the current density as obtained from the mean-field methods reaches the space-charge-limited current (SCLC) density and stays constant for negative Φ, whereas the 3D KMC simulations show that the SCLC condition is actually only well approached around $\Phi = 0.3$ eV. The difference is not caused by possible oversimplifications when using a 1D DD model, as 3D ME modeling leads to essentially the same discrepancy.

In order to understand the unusual current density at small and negative Φ, we investigate the average hole concentration per molecular site obtained from the three simulation methods in Figs. 1(b) and 1(c), for the first and second layer adjacent to the interface, respectively. The results of the 1D DD and 3D ME simulations are similar: the hole concentration continues to increase towards small and negative Φ, as expected in the conventional mean-field injection theory. The results of the 3D KMC simulations, however, show a larger hole concentration in the first layer and a smaller hole concentration in the second layer. In particular, the hole concentration in the second layer decreases significantly at negative Φ, and follows a trend that is similar to that in the current density.

We attribute the observed dependence of the current density on the nominal injection barrier to the Coulomb repulsion between the charge carriers in the first layer, the Coulomb attraction between the injected charge carriers in OS and their image charges in the electrode (forming

interfacial dipoles), and the Coulomb repulsion impeding charge carriers being further injected into the second layer of molecular sites nearby. These short-range intermolecular Coulomb interactions are included in an exact manner in the 3D KMC simulations, but only treated using the mean-field approximation within the 3D ME and 1D DD simulations. The image-force-stabilized interfacial dipole layer leads to a larger hole concentration in the first layer, and at the same time results in a reduced hole concentration in the second layer. This can explain the current-density reduction towards smaller and negative Φ. The 3D KMC simulation results suggest that charges can less easily escape from the metal-OS interface than as expected from mean-field simulations. Within mean-field simulations the ease of escape of a specific hole from the interface layer is too large because (i) the layer-averaged surface charge density and potential incorrectly contain a contribution from that hole itself ("self-energy"), and (ii) the hole will actually be surrounded by a region with a reduced charge density ("Coulomb hole"). The distance dependence of the pair correlation of the charge carriers in the first layer is quantified in Figs. S3(a) and (b) and Fig. S4 within the Supplemental Material [42], and the spatial distribution is visualized in Figs. S3(c)–(f) and Fig. S5 within the Supplemental Material. A similarly reduced escape rate is also found from 3D KMC simulations of the accumulated charge density near an internal potential barrier in an OS device [43].

In Fig. 2, we show the layer-averaged hole-concentration profile for the entire device, as calculated from the three simulation methods. At large positive Φ, the results from the 1D DD, 3D ME, and 3D KMC simulations are very similar. While the 1D DD similations yield a continuous hole concentration, the inclusion of energetic disorder in the 3D ME and 3D KMC simulations is seen to lead to fluctuations of the layer-averaged hole concentration. At small and negative Φ, the hole concentration is reduced in the second layer (as shown already in Fig. 1), but also beyond that layer. That explains why charge injection becomes then inefficient and the current density is reduced.

In order to further study how the injection process is hampered by the Coulomb interaction between the charge carriers in the interfacial dipole layer, we study the sensitivity of the effect to various simulation parameters. Figure 3 shows that the effect becomes stronger with decreasing energetic disorder (a), when the relative effect of Coulomb interactions on the site energies increases, and with decreasing temperature (b), when thermal activation less efficiently competes with the Coulomb repulsion. The effect decreases with increasing ε_r, so that the Coulomb interaction is reduced, and vanishes almost for $\varepsilon_r \sim 10$ (c). No strong dependence of $J(\Phi)$ on λ is observed, apart from an overall shift due to the variation of the mobility with λ (d). We furthermore find that the effect decreases with increasing voltage, as a large applied field can unblock the

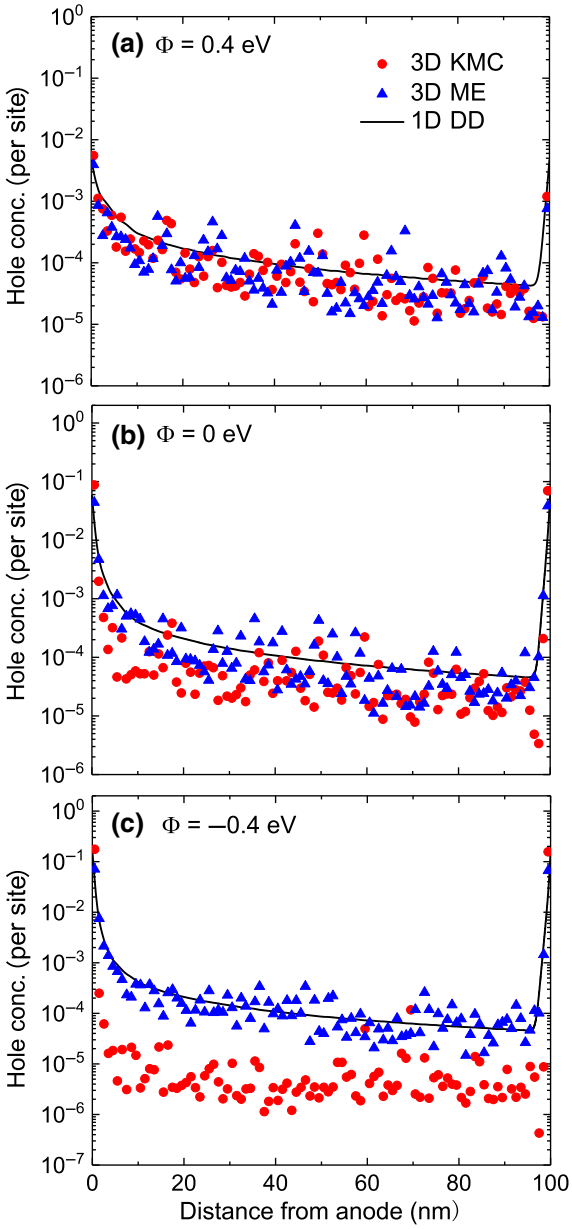

FIG. 2. Hole-concentration profile of the devices studied in Fig. 1, obtained for various nominal injection barriers Φ using 3D KMC, 3D ME, and 1D DD simulations.

charges in the high-density zone, and with increasing layer thickness, when interfacial effects become less relevant. These simulation results are shown in Sec. S3 (Fig. S6) within the Supplemental Material [42].

Figure 4 shows the effect of Coulomb interactions on the layer-averaged DOS and the layer-averaged density of occupied states (DOOS) in the image-force-stabilized interfacial dipole layer, obtained from 3D KMC simulations, for three values of Φ. Figures S7(a)–(f) in Sec. S4 of the Supplemental Material [42] gives simulation results for intermediate values of Φ. The dotted curves give the Gaussian DOS, with a width $\sigma = 0.1$ eV, before charge

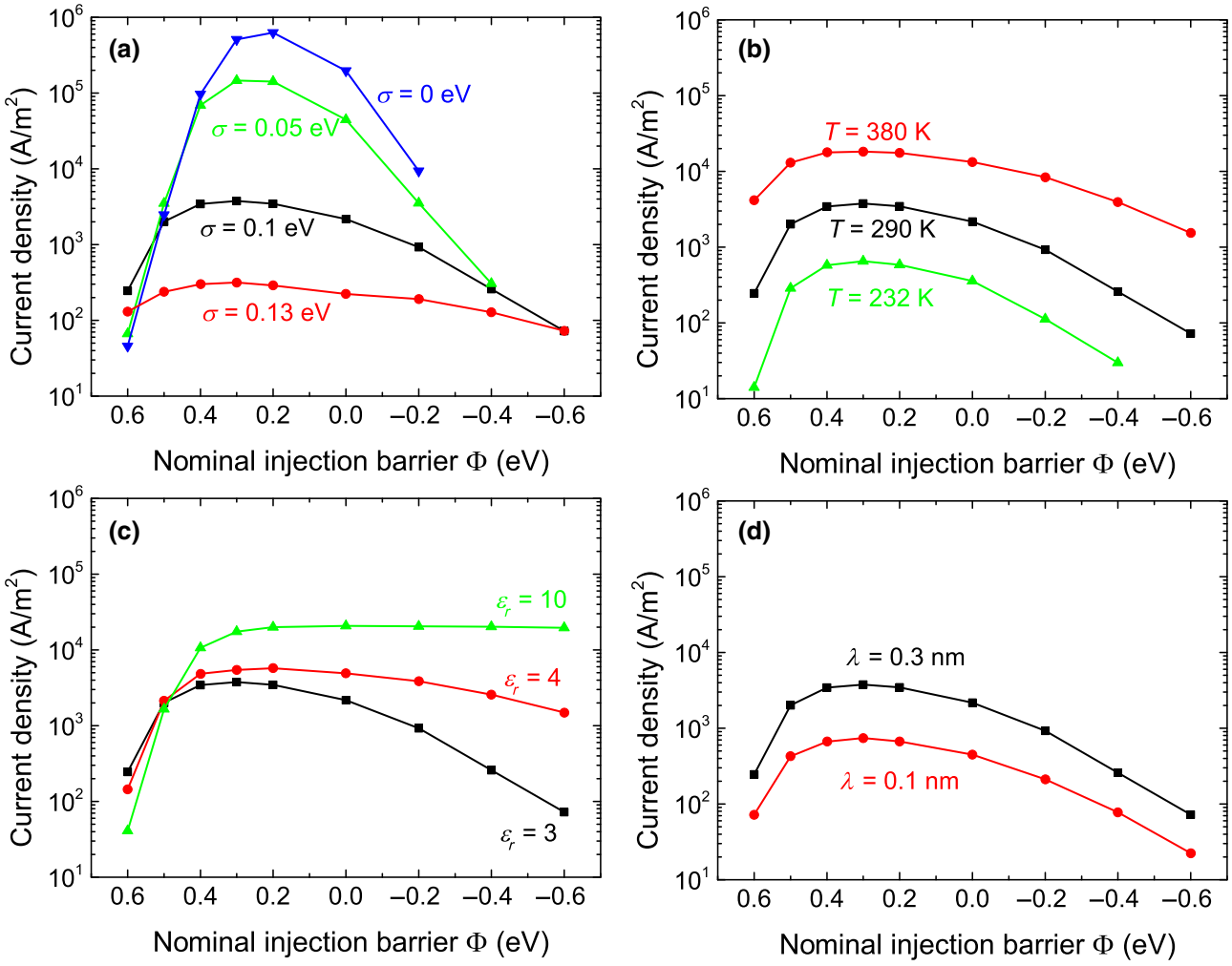

FIG. 3. Dependence of the current density on the nominal injection barrier Φ as obtained from 3D KMC simulations for the devices studied in Fig. 1 at various values of (a) energetic disorder width σ, (b) temperature T, (c) relative dielectric constant ε_r, and (d) wave-function decay length λ. The black curves give the simulation results for the nominal parameter values, listed in Table I.

injection and excluding the image potential effect. The DOS is given as a function of the energy $E - E_F$ that is required for transferring a hole from a site with energy E to the metal Fermi level, and is centered at the energy $E - E_F = -\Phi$. The part of the DOS that would under these conditions be occupied by the density of holes that resides in the first layer (DOOS) is indicated as a filled black peak. The full curves show the DOS after including the Coulomb interaction with the holes in the organic semiconductor and the image-charge interaction. The latter effect leads, within our model for the nth layer, to a stabilizing (positive) energy shift equal to $\Delta E_{\rm im}(n) \approx +0.12/n$ eV. The DOOS for the first layer is indicated as a filled red-colored peak.

Figure 4(a) shows that for a nominal injection barrier of 0.4 eV the unoccupied DOS is for all layers almost equal to that for the reference (dotted curve). The upward shift due to the image-charge interaction is for each layer then quite well balanced by the downward shift due to the Coulomb repulsion between the holes. However, the plot of the DOOS (see the inset, log scale) shows that for the occupied states in the first layer these shifts are not equal. The reference DOOS peak (black), which follows from filling the Gaussian DOS with a concentration of approximately 5.5×10^{-3} holes [see Fig. 1(b)], is located at about +0.28 eV with respect to the peak of the DOS at −0.4 eV, whereas the actual DOOS peak (red) is located at about 0 eV. Due to the relatively small hole density in the OS the effect of the hole-hole Coulomb repulsion is in this case relatively small, so that the upward shift due to the image-charge interaction prevails. Figures 4(b) and 4(c) show that the situation is quite different when there is no injection barrier or when Φ is even negative, so that there is a much larger hole density near the interface. For the unoccupied states, the DOS shows now a significant shift to more negative energies, resulting from the stronger hole-hole

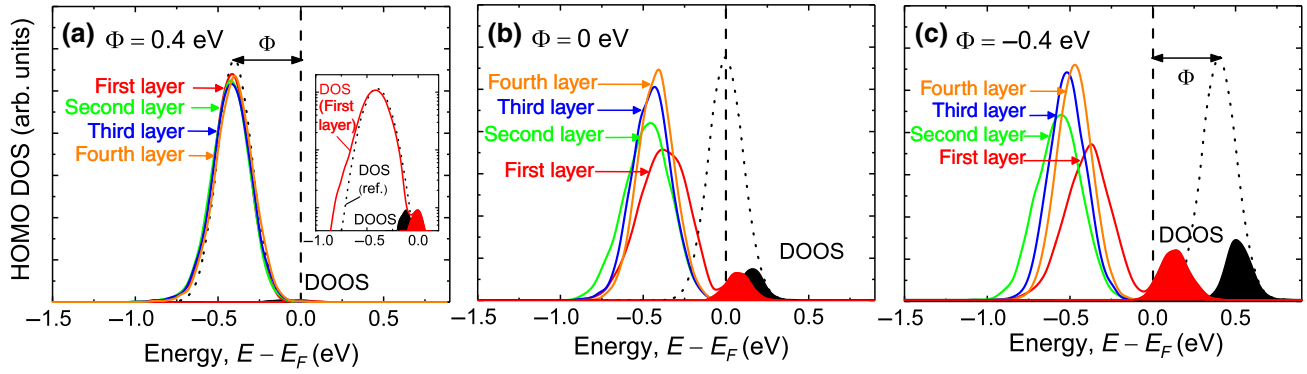

FIG. 4. (a)–(c) Layer-resolved distribution of molecular site energies near the injecting electrode from 3D KMC simulations for three values of Φ, for the devices studied in Fig. 1. The filled peaks give the DOOS with (red) and without (black) Coulombic effects for the first layer near the electrode. Dotted curves: bulk DOS before charge injection. Results for an extended set of Φ values are given in Sec. S4 [Figs. S7(a)–(f)] of the Supplemental Material [42]. The inset figure in (a) shows the DOS in a logarithmic scale.

Coulomb repulsion. The effect is only compensated in part by the positive-energy shift due to the image-charge interaction, which is strongest for the first layer. A shift to more negative energies is also seen for the DOOS of the first layer. However, due to a spatially correlated distribution of the holes in the first layer ("Coulomb hole formation," see Figs. S3 and S5 within the Supplemental Material [42]), that shift is much smaller than the DOS shift.

When Φ becomes more negative, the DOS of the first layer shows to an increasing extent a double-peaked structure, reflecting a Coulomb correlation effect. The simulations also reveal then a decrease of the overlap between the distributions of occupied states in the first layer and the empty states in the other layers. Escape from the first layer becomes then more difficult. For example, the distance of the DOOS peak for the first layer to the DOS peak for the second layer increases gradually from about 0.41 eV ($\Phi = 0.4$ eV) to 0.76 eV ($\Phi = -0.6$ eV). We therefore regard the observation of a maximum in the current density for Φ close to 0.2 eV as the combined result of, on the one hand, an increase of the charge density in the first layer with decreasing Φ and on the other hand an increase of the energy barrier for charge transfer from the first layer to the next layers.

B. Effect of thin interlayers

We next investigate the effect of thin interlayers at the metal-OS interfaces. Figure 5 contains the results of 3D KMC simulations for devices studied in Fig. 1, with interlayers with various layer thicknesses and HOMO energies that is shifted with respect to that of the OS. As shown by (a), the insertion of a 1–2 nm interlayer with a HOMO energy offset of $\Delta E = 0.2$ eV leads already to an extension of the SCLC regime to strongly negative nominal injection barriers. For $\Phi = -0.6$ eV, a 2-nm interlayer leads to an increase of the current density by approximately a factor of 50. The contact is then perfectly Ohmic. For thicker interlayers, the Φ window for which SCLC conditions are accomplished decreases gradually. Figure 5(b) shows that also 2-nm interlayers with a larger offset energy can be used, as long as the metal-interlayer injection barrier $\Phi + \Delta E$ is smaller than approximately 0.4 eV. The hole density in the first layer remains then sufficiently high. For a negative HOMO energy offset, the interlayer becomes a trapping region for injected holes. The figure shows, for $\Delta E = -0.05$ eV, that the injection efficiency is then strongly reduced.

The interlayer effect may be understood from a similar analysis as shown in Fig. 4. The reduced charge density in the interlayer gives rise to a reduced negative energy shift of the distribution of unoccupied site energies of the third layer (the first OS layer), which now overlaps with the distribution of occupied site energies in the first layer. This greatly facilitates charge transport to the third layer, resulting in an enhancement of the current density. The variation of the layer-resolved site energy distribution when varying Φ or ΔE is shown by Figs. S7(g)–(i) and Fig. S8 within the Supplemental Material [42], respectively. We find that to achieve SCLC conditions, only an interlayer at the injecting electrode is needed. The effect on J of removing the interlayer at the extracting electrode is found to be very small (see Fig. S9 within the Supplemental Material [42]).

The calculated sensitivity to ΔE is qualitatively consistent with the experimental observations presented in Ref. [11]. However, the optimum thickness is somewhat smaller than the range of 3–5 nm observed in Ref. [11] for systems with MoO_3 electrodes. The difference might be related to a deviating disorder width near the electrode, as suggested in Ref. [11], or due to realistic thickness variations of the interlayer. We find for systems with a 2-nm thickness variation a shift of the optimum thickness from

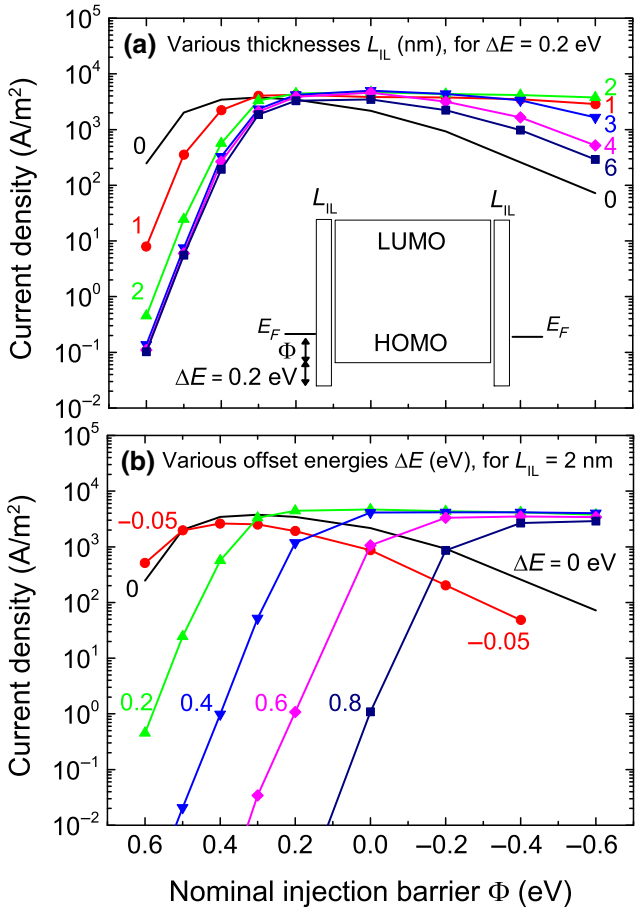

FIG. 5. 3D KMC simulation results of the effect of interlayers [see the inset in (a)] on the current density in the devices studied in Fig. 1, as a function of the nominal injection barrier Φ. (a) Dependence of $J(\Phi)$ on the interlayer thickness L_{IL} for $\Delta E =$ 0.2 eV. (b) Dependence of $J(\Phi)$ on ΔE for $L_{IL} = 2$ nm.

2 to 3 nm (see Fig. S10 in Sec. S5 of the Supplemental Material [42]).

We note that in our simulations no direct transfer from the electrode to more distant layers is included. When including such an effect, the use of interlayers with a large offset energy ΔE is expected to become less disadvantageous.

IV. CONCLUSIONS AND OUTLOOK

In summary, we show that the current density in metal-OS-metal devices with small or even negative nominal metal-OS injection barriers can be significantly injection limited. The analysis of the results of 3D KMC simulations shows that the effect is due to the Coulomb interaction between the injected charge carriers in the interfacial dipole layer and with their image charges in the electrode. Our work provides an alternative and more generic explanation for the findings reported in Ref. [11] concerning the difficulty of obtaining Ohmic injection for nominally barrier-free devices and concerning the functioning a thin interlayer that can successfully extend the barrier range for which Ohmic injection is possible. Our work therefore emphasizes the significance of using interlayers when studying the energetic disorder and the mobility function of organic semiconductors using SCLC measurements.

We regard the 3D KMC simulation method that has been used in this work as the most obvious next step beyond conventional mean-field simulations, using, e.g., a 1D DD approach. However, it is not fully evident that a description of the injection process in terms of the hopping of charges that are localized on a lattice of point sites is also appropriate in regions where the charge-carrier density is very high, such as near well-injecting electrodes. In particular, one may ask whether under such conditions the dielectrically screened Coulomb-type charge-charge interaction that has been assumed in this work provides a sufficiently accurate approximation and to what extent the assumed localized nature of the highest-energy occupied hole states remains valid. Studies of the doping dependence of the conductivity of conjugated polymers, e.g., have provided evidence of a growing delocalization with increasing state filling [44]. Furthermore, the electronic structure of molecular layers that are in direct contact with a clean elemental metal or alloy surface can be influenced by weak covalent interactions [45]. It is therefore of interest to extend our studies in future work by performing quantum-chemical calculations of the charge dynamics near a metal-OS interface. It would be of interest as well to investigate possible limitations of the image-charge model, by studying the dynamics of the dielectric response in pure metal and compound electrodes such as metallic transition-metal oxides. As next steps, we also suggest that noise measurements could be used to experimentally probe the role of the interfacial dipole layer [46], and that it is of interest to study its possible effect on the conductivity of molecularly doped organic semiconductors that are used extensively as injection layers in organic semiconductor devices [13–15].

ACKNOWLEDGMENTS

This work is supported by the National Key Research and Development Program of China (No. 2017YFB 0404404), Science and Technology Program of Guangzhou (No. 2019050001), the leading talents of Guangdong Province Program (No. 00201504), Program for Chang Jiang Scholars and Innovative Research Teams in Universities (No. IRT_17R40), Guangdong Provincial Key Laboratory of Optical Information Materials and Technology (No. 2017B030301007), National Center for International Research on Green Optoelectronics, MOE International Laboratory for Optical Information Technologies and the 111 Project, and the Grant of 2019 Guangdong Recruitment Program of Foreign Experts (No. 191900017).

[1] L. S. Hung, C. W. Tang, and M. G. Mason, Enhanced electron injection in organic electroluminescence devices using an Al/LiF electrode, Appl. Phys. Lett. **70**, 152 (1997).

[2] J. C. Scott and G. G. Malliaras, Charge injection and recombination at the metal–organic interface, Chem. Phys. Lett. **299**, 115 (1999).

[3] S. Barth, U. Wolf, H. Bässler, P. Müller, H. Riel, H. Vestweber, P. F. Seidler, and W. Rieß, Current injection from a metal to a disordered hopping system. III. Comparison between experiment and monte carlo simulation, Phys. Rev. **60**, 8791 (1999).

[4] E. Tutiš, M.-N. Bussac, and L. Zuppiroli, Image force effects at contacts in organic light-emitting diodes, Appl. Phys. Lett. **75**, 3880 (1999).

[5] Y. Shen, M. W. Klein, D. B. Jacobs, J. C. Scott, and G. G. Malliaras, Mobility-Dependent Charge Injection Into an Organic Semiconductor, Phys. Rev. Lett. **86**, 3867 (2001).

[6] M. A. Baldo and S. R. Forrest, Interface-limited injection in amorphous organic semiconductors, Phys. Rev. B **64**, 085201 (2001).

[7] F. Neumann, Y. A. Genenko, C. Melzer, S. V. Yampolskii, and H. von Seggern, Self-consistent analytical solution of a problem of charge-carrier injection at a conductor/insulator interface, Phys. Rev. B **75**, 205322 (2007).

[8] L. Li, G. Meller, and H. Kosina, Diffusion-controlled charge injection model for organic light-emitting diodes, Appl. Phys. Lett. **91**, 172111 (2007).

[9] J. J. M. van der Holst, M. A. Uijttewaal, B. Ramachandhran, R. Coehoorn, P. A. Bobbert, G. A. de Wijs, and R. A. de Groot, Modeling and analysis of the three-dimensional current density in sandwich-type single-carrier devices of disordered organic semiconductors, Phys. Rev. B **79**, 085203 (2009).

[10] Y. A. Genenko, S. V. Yampolskii, C. Melzer, K. Stegmaier, and H. von Seggern, Charge carrier injection into insulating media: Single-particle versus mean-field approach, Phys. Rev. B **81**, 125310 (2010).

[11] N. B. Kotadiya, H. Lu, A. Mondal, Y. Ie, D. Andrienko, P. W. M. Blom, and G.-J. A. H. Wetzelaer, Universal strategy for ohmic hole injection into organic semiconductors with high ionization energies, Nat. Mater. **17**, 329 (2018).

[12] N. B. Kotadiya, A. Mondal, S. Xiong, P. W. M. Blom, D. Andrienko, and G.-J. A. H. Wetzelaer, Rigorous characterization and predictive modeling of hole transport in amorphous organic semiconductors, Adv. Electr. Mater. **4**, 1800366 (2018).

[13] M. Pfeiffer, S. R. Forrest, K. Leo, and M. E. Thompson, Electrophosphorescent p–i–n organic light emitting devices for very high efficiency flat panel displays, Adv. Mater. **14**, 1633 (2002).

[14] B. Lüssem, M. Riede, and K. Leo, Doping of organic semiconductors, Phys. Stat. Sol. (a) **210**, 9 (2013).

[15] M. Schwarze, C. Gaul, R. Scholz, F. Bussolotti, A. Hofacker, K. S. Schellhammer, B. Nell, B. D. Naab, Z. Bao, D. Spoltore, K. Vandewal, J. Widmer, S. Kera, N. Ueno, F. Ortmann, and K. Leo, Molecular parameters responsible for thermally activated transport in doped organic semiconductors, Nat. Mater. **18**, 242 (2019).

[16] I. G. Hill, A. Rajagopal, A. Kahn, and Y. Hu, Molecular level alignment at organic semiconductor-metal interfaces, Appl. Phys. Lett. **73**, 6629 (1998).

[17] H. Ishii, K. Sugiyama, E. Ito, and K. Seki, Energy level alignment and interfacial electronic structures at organic/metal and organic/organic interfaces, Adv. Mater. **11**, 605 (1999).

[18] S. Braun, W. R. Salaneck, and M. Fahlman, Energy-level alignment at organic/metal and organic/organic interfaces, Adv. Mater. **21**, 1450 (2009).

[19] J. Hwang, A. Wan, and A. Kahn, Energetics of metal-organic interfaces: New experiments and assessment of the field, Mater. Sci. Eng. R **64**, 1 (2009).

[20] I. Lange, J. C. Blakesley, J. Frisch, A. Vollmer, N. Koch, and D. Neher, Band Bending in Conjugated Polymer Layers, Phys. Rev. Lett. **106**, 216402 (2011).

[21] M. T. Greiner, M. G. Helander, W. M. Tang, Z. B. Wang, J. Qiu, and Z. H. Lu, Universal energy-level alignment of molecules on metal oxides, Nat. Mater. **11**, 76 (2012).

[22] J. C. Blakesley and N. C. Greenham, Charge transfer at polymer-electrode interfaces: The effect of energetic disorder and thermal injection on band bending and open-circuit voltage, J. Appl. Phys. **106**, 034507 (2009).

[23] P. C. Rusu, G. Giovannetti, C. Weijtens, R. Coehoorn, and G. Brocks, First-principles study of the dipole layer formation at metal-organic interfaces, Phys. Rev. B **81**, 125403 (2010).

[24] L. Ley, Y. Smets, C. I. Pakes, and J. Ristein, Calculating the universal energy-level alignment of organic molecules on metal oxides, Adv. Funct. Mater. **23**, 794 (2013).

[25] M. Oehzelt, N. Koch, and G. Heimel, Organic semiconductor density of states controls the energy level alignment at electrode interfaces, Nat. Commun. **5**, 4174 (2014).

[26] M. Mochena and M. Pollak, Low-Temperature Properties of Interacting Particles in Disordered Media: A Method with Application to Coulomb Glass, Phys. Rev. Lett. **67**, 109 (1991).

[27] E. R. Grannan and C. C. Yu, Critical Behavior of the Coulomb Glass, Phys. Rev. Lett. **71**, 3335 (1993).

[28] J. Zhou, Y. C. Zhou, J. M. Zhao, C. Q. Wu, X. M. Ding, and X. Y. Hou, Carrier density dependence of mobility in organic solids: A Monte Carlo simulation, Phys. Rev. B **75**, 153201 (2007).

[29] F. Liu, H. van Eersel, B. Xu, J. G. E. Wilbers, M. P. de Jong, W. G. van der Wiel, P. A. Bobbert, and R. Co-ehoorn, Effect of Coulomb correlation on charge transport in disordered organic semiconductors, Phys. Rev. B **96**, 205203 (2017).

[30] A. Sharma, F. W. A. van Oost, M. Kemerink, and P. A. Bobbert, Dimensionality of charge transport in organic field-effect transistors, Phys. Rev. B **85**, 235302 (2012).

[31] H. Bässler, Charge transport in disordered organic photoconductors a Monte Carlo simulation study, Phys. Stat. Sol. (b) **175**, 15 (1993).

[32] M. Mesta, M. Carvelli, R. J. de Vries, H. van Eersel, J. J. M. van der Holst, M. Schober, M. Furno, B. Lüssem, K. Leo, P. Loebl, R. Coehoorn, and P. A. Bobbert, Molecular-scale simulation of electroluminescence in a multilayer white organic light-emitting diode, Nat. Mater. **12**, 652 (2013).

[33] The 3D-KMC tool used in this work is Bumblebee, provided by Simbeyond B.V. (simbeyond.com).

[34] Z. G. Yu, D. L. Smith, A. Saxena, R. L. Martin, and A. R. Bishop, Molecular geometry fluctuations and field-dependent mobility in conjugated polymers, Phys. Rev. B **63**, 085202 (2001).

[35] W. F. Pasveer, J. Cottaar, C. Tanase, R. Coehoorn, P. A. Bobbert, P. W. M. Blom, D. M. de Leeuw, and M. A. J. Michels, Unified Description of Charge-Carrier Mobilities in Disordered Semiconducting Polymers, Phys. Rev. Lett. **94**, 206601 (2005).

[36] J. S. Bonham and D. H. Jarvis, A new approach to space-charge-limited conduction theory, Austr. J. Chem. **30**, 705 (1977).

[37] S. L. M. van Mensfoort and R. Coehoorn, Determination of Injection Barriers in Organic Semiconductor Devices from Capacitance Measurements, Phys. Rev. Lett. **100**, 086802 (2008).

[38] A. Miller and E. Abrahams, Impurity conduction at low concentrations, Phys. Rev. **120**, 745 (1960).

[39] J. J. M. van der Holst, F. W. A. van Oost, R. Coehoorn, and P. A. Bobbert, Monte carlo study of charge transport in organic sandwich-type single-carrier devices: Effects of Coulomb interactions, Phys. Rev. B **83**, 085206 (2011).

[40] Y. Roichman, Y. Preezant, and N. Tessler, Analysis and modeling of organic devices, Phys. Stat. Sol. (a) **201**, 1246 (2004).

[41] P. R. Emtage and J. J. O'Dwyer, Richardson-Schottky Effect in Insulators, Phys. Rev. Lett. **16**, 365 (1966).

[42] See the Supplemental Material at http://link.aps.org/supplemental/10.1103/PhysRevApplied.17.024003 for additional information on the simulation methods, sensitivity analyses, site-resolved distributions of charge carriers, layer-resolved distributions of site energies, and simulations for special devices.

[43] J. Cottaar, R. Coehoorn, and P. A. Bobbert, Modeling of charge transport across disordered organic heterojunctions, Organ. Electr. **13**, 667 (2012).

[44] H. C. F. Martens, I. N. Hulea, I. Romijn, H. B. Brom, W. F. Pasveer, and M. A. J. Michels, Understanding the doping dependence of the conductivity of conjugated polymers: Dominant role of the increasing density of states and growing delocalization, Phys. Rev. B **67**, 121203 (2003).

[45] H. Vázquez, R. Oszwaldowski, P. Pou, J. Ortega, R. Pérez, F. Flores, and A. Kahn, Dipole formation at metal/PTCDA interfaces: Role of the charge neutrality level, Europhys. Lett. **65**, 802 (2004).

[46] T. González, C. González, J. Mateos, D. Pardo, L. Reggiani, O. M. Bulashenko, and J. M. Rubí, Universality of the 1/3 Shot-Noise Suppression Factor in Nondegenerate Diffusive Conductors, Phys. Rev. Lett. **80**, 2901 (1998).